PHILOSOPHICAL TRANSACTIONS A

royalsocietypublishing.org/journal/rsta

Research

**Cite this article:** Galenko PK, Ankudinov V, Reuther K, Rettenmayr M, Salhoumi A, Kharanzhevskiy EV. 2019 Thermodynamics of rapid solidification and crystal growth kinetics in glass-forming alloys. *Phil. Trans. R. Soc. A* **377**: 20180205.
http://dx.doi.org/10.1098/rsta.2018.0205

Accepted: 12 December 2018

One contribution of 17 to a theme issue 'Heterogeneous materials: metastable and non-ergodic internal structures'.

**Subject Areas:**
materials science, solid state physics, thermodynamics

**Keywords:**
fast transformations, rapid solidification, growth of crystals, glass transition

**Author for correspondence:**
M. Rettenmayr
e-mail: m.rettenmayr@uni-jena.de

# Thermodynamics of rapid solidification and crystal growth kinetics in glass-forming alloys

P. K. Galenko[1], V. Ankudinov[2,3], K. Reuther[1], M. Rettenmayr[1], A. Salhoumi[4] and E. V. Kharanzhevskiy[2]

[1]Faculty of Physics and Astronomy, Otto Schott Institute of Materials Research, Friedrich-Schiller-Universität-Jena, 07743 Jena, Germany
[2]Department of Physics and Energetics, Laboratory of Condensed Matter Physics, Udmurt State University, 426034 Izhevsk, Russia
[3]Department of Theoretical and Mathematical Physics, Laboratory of Multi-Scale Mathematical Modeling, Ural Federal University, 620000 Ekaterinburg, Russia
[4]Faculté des Sciences Ben M'Sik, Laboratoire de Physique de la Matière Condensée (LPMC), Université Hassan II de Casablanca, BP 7955 Casablanca, Morocco

PKG, 0000-0003-2941-7742; MR, 0000-0003-4721-5087

Thermodynamic driving forces and growth rates in rapid solidification are analysed. Taking into account the relaxation time of the solute diffusion flux in the model equations, the present theory uses, in a first case, the deviation from local chemical equilibrium, and ergodicity breaking. The second case of ergodicity breaking may exist in crystal growth kinetics of rapidly solidifying glass-forming metals and alloys. In this case, a theoretical analysis of dendritic solidification is given for congruently melting alloys in which chemical segregation does not occur. Within this theory, a deviation from thermodynamic equilibrium is introduced for high undercoolings via gradient flow relaxation of the phase field. A comparison of the present derivations with previously verified theoretical predictions and experimental data is given.

This article is part of the theme issue 'Heterogeneous materials: metastable and non-ergodic internal structures'.

THE ROYAL SOCIETY PUBLISHING

# 1. Introduction

Rapid solidification can be initiated by fast quenching or slow cooling to avoid premature nucleation and to attain deep undercoolings. Cooling rates may reach $10^6\,(\mathrm{K\,s^{-1}})$ for melt spinning, or atomization by gas, impulse or in a drop tube; temperature gradients can reach $10^9\,(\mathrm{K\,m^{-1}})$ in laser annealing, and undercoolings of up to 300–500 (K) can be achieved (see refs. [1–6] for details of techniques and measurements). Such large driving forces lead to solidification rates in the order of several tens of metres per second [5,7]. Considering that the characteristic diffusion speed is in the order of several metres or tens of metres per second in metallic alloys and of several centimetres or tens of centimetres per second in semiconductors [8], it becomes obvious that the solid/liquid interface may exhibit velocities in the order of or even larger than the diffusion speed. In such a case, the rapid solidification front may undergo diffusionless (chemically partitionless) transformation which may proceed in a wide or narrow interval of driving forces [3,4,9,10].

Progress in the formulation of the thermodynamical basis [11–16] has led to an extended description [17] going beyond the hypothesis of local equilibrium that is stipulated by broken ergodicity in rapidly solidifying samples [18]. Using a local non-equilibrium model of dendritic growth [19], the kinetics of rapid solidification in slowly and deeply undercooled samples has been described consistently using experimental data on the solidification kinetics of a number of interstitial and substitutional solution phases during dendritic growth [20–23]. In these studies, it was shown that the interface velocity monotonically increases with undercooling (even though specific peculiarities in the transition from diffusion limited to thermally controlled growth of dendrites were found). Rapid kinetics with an unusually steep dendrite velocity/undercooling relationship has also been obtained in intermetallic alloys with an order–disorder transition [24, 25]. However, the velocity of dendrites in melts of intermetallic phases also exhibited a monotonic increase with increasing undercooling. Another type of velocity/undercooling relationship can be experimentally found in the kinetics of dendritic solidification of glass-forming metals and alloy melts. For glass-forming samples produced from metals, alloys, oxides, organics or chalcogenides [26–28], the growth rate has a maximum value at a defined undercooling that lies between the glass-transition undercooling and zero undercooling directly at the melting (or liquidus) temperature. Moreover, for the alloy $Cu_{50}Zr_{50}$ (concentrations in %), a transition from purely thermodynamic to kinetically controlled growth has been experimentally observed for the first time [27]. Attempts to describe such transitions using common dendrite growth theory [29] lead to a smooth and gradual behaviour of velocity versus undercooling, describing the main part of the experimental data well, but overestimating velocities at the highest undercooling where the so-called 'abrupt drop in kinetics' occurs. The thermodynamic and kinetic analysis of the solidification behaviour in glass-forming samples is the main goal of the present paper.

The article is divided into two main parts. In the first part (§§2 and 3), we analyse thermodynamic driving forces and growth rates in dendritic rapid solidification and compare them with previously verified theoretical predictions. Here the solidification can be considered a rapid process if the solid/liquid interface moves with a velocity comparable to the diffusion speed in the bulk liquid. In this case, the relaxation time of the solute diffusion flux is not negligible and should be included in the model equations that characterize deviations from local equilibrium and ergodicity breaking [18]. The second part of the article is devoted to the analysis of dendritic solidification of congruently melting alloys in which the chemical composition does not influence the growth velocity due to the absence of chemical segregation. A dendrite growth model for predicting the solidification kinetics of glass-forming alloys is formulated in §4. The model consists of a system of equations describing (i) the undercooling balance at the dendritic surface, (ii) the stability condition for the dendrite tip at arbitrary growth Péclet numbers, and (iii) the kinetic contribution following on from the travelling wave solution of the phase field model (see appendices). In this case, we also deal with rapid solidification considering that gradient

flow relaxation is used in the model equations describing the deviation from local equilibrium and ergodicity breaking [18].

## 2. Entropy change in rapid solidification

Consider a solidifying sample of a volume $v_0$ of a binary alloy. The concentration distribution of solute is given by $C(x,t)$, and at the interface the concentrations are $C_L^*$ in the liquid phase and $C_S^*$ in the solid phase. The temperature $T$ of the sample is constant and the total pressure tensor $\boldsymbol{P}$ is related to the viscous pressure $\boldsymbol{P}^\nu$ by $\boldsymbol{P}=p\boldsymbol{U}+\boldsymbol{P}^\nu$, where $p$ is the equilibrium (static) pressure and $\boldsymbol{U}$ the identity tensor. As usual, $\boldsymbol{P}^\nu$ is split into two parts, a bulk pressure $p^\nu=\frac{1}{3}\mathrm{trace}\,\boldsymbol{P}^\nu$ and a deviatoric part $\widehat{\boldsymbol{P}}^\nu$, so that

$$\boldsymbol{P}=p\boldsymbol{U}+p^\nu\boldsymbol{U}+\widehat{\boldsymbol{P}}^\nu. \tag{2.1}$$

The necessity of the pressure introduction is dictated by (i) accumulated stresses around rapidly moving interface and (ii) the difference in density of the liquid and solid leading to shrinkage effects. For example, an increasing dislocation density in the microstructure of alloys with increasing solidification rate [30] directly testifies that rapid solidification results in an accumulation and relaxation of stresses.

### (a) The bulk entropy

The temporal evolution of the concentration field follows from the formalism of extended irreversible thermodynamics (EIT) [31,32]. The total entropy of the entire system of the volume $v_v$ is described by

$$-TS(t)=\int_{v_v}[\mu_A C_A+\mu_B C_B+\alpha_A J_A^2+\alpha_B J_B^2+\alpha_{\mathbf{P}}:\mathbf{P}]\,\mathrm{d}v_v, \tag{2.2}$$

where $C_A$ is the concentration of the $A$-atoms having the chemical potential $\mu_A$, $C_B$ is the concentration of the $B$-atoms having the chemical potential $\mu_B$, $J_A$ and $J_B$ are the diffusion fluxes of the $A$- and $B$-atoms, respectively. The thermodynamic coefficients $\alpha_A$ and $\alpha_B$ are defined by

$$\alpha_A=\frac{\tau_D^{(A)}}{D^{(A)}}\frac{\partial\mu_A}{\partial C_A}=\frac{1}{(V_D^{(A)})^2}\frac{\partial\mu_A}{\partial C_A},\quad \alpha_B=\frac{\tau_D^{(B)}}{D^{(B)}}\frac{\partial\mu_B}{\partial C_B}=\frac{1}{(V_D^{(B)})^2}\frac{\partial\mu_B}{\partial C_B}, \tag{2.3}$$

where $\tau_D^{(A)}$ and $\tau_D^{(B)}$ are the relaxation times of the diffusion fluxes, $J_A$ and $J_B$, respectively, $D^{(A)}$ and $D^{(B)}$ the diffusion coefficients of the $A$- and $B$-atoms, respectively, and $V_D^{(A)}=(D^{(A)}/\tau_D^{(A)})^{1/2}$ and $V_D^{(B)}=(D^{(B)}/\tau_D^{(B)})^{1/2}$ are the maximum speeds for diffusion of the $A$- and $B$-atoms, respectively.

Using the expression for the pressure (2.1) and the respective expression for $\alpha_{\mathbf{P}}$ (see [31,32]), the entropy (2.2) can be re-written as

$$-TS(t)=\int_{v_v}[\mu_A C_A+\mu_B C_B+\alpha_A J_A^2+\alpha_B J_B^2-pv+v\alpha_0(p^\nu)^2+v\alpha_2\widehat{\mathbf{P}}^\nu:\widehat{\mathbf{P}}^\nu]\,\mathrm{d}v_v, \tag{2.4}$$

where the thermodynamic coefficients $\alpha_0=\zeta_B^{-1}$ and $\alpha_2=(2\eta_S)^{-1}$ are defined by the bulk viscosity $\zeta_B$ and shear viscosity $\eta_S$, respectively.

We use the concentration definitions $C=C_B=1-C_A$ together with the fluxes $J_D=-J_A=J_B$, $J_D^2=J_A^2=J_B^2$. Then, considering further only a semi-infinite one-dimensional solidification domain, equation (2.2) simplifies to

$$S(x,t)=\int_0^\infty[s_{\mathrm{eq}}(x,t)+s_{\mathrm{ne}}(x,t)]\,\mathrm{d}x, \tag{2.5}$$

where the local equilibrium part of the entropy density is

$$-Ts_{\mathrm{eq}}(x,t)=\mu_A(1-C)+\mu_B C-pv, \tag{2.6}$$

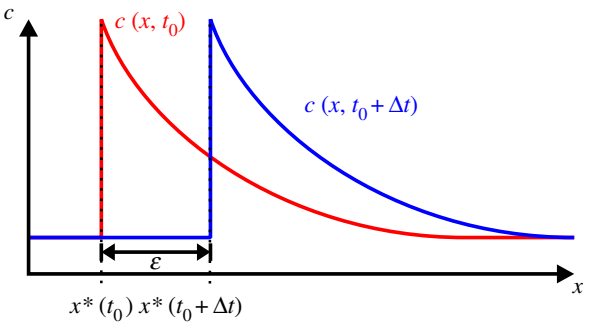


**Figure 1.** Two snapshots of the concentration distribution at a solidification front, separated by a small time step $\Delta t$, where the interface has the position $x^*$ and moves with a constant velocity $V$ to the right of the figure. (Online version in colour.)

and the local non-equilibrium part of the entropy density is

$$-Ts_{\mathrm{ne}}(x,t) = \alpha_D J_D^2 + v\alpha_0 (p^v)^2 + v\alpha_2 (P_{xx}^v)^2, \tag{2.7}$$

with $\alpha_D = \alpha_A + \alpha_B$ and $P_{xx}^v$ the component of viscous pressure along the $x$-axis.

## (b) Entropy produced by the moving interface

Neglecting the diffusion processes in the solid phase, $J_D(x,t) = 0 : x < x^*(t)$, where $x^*(t)$ is the position of the solid/liquid interface, consider now the change of entropy in the entire system caused by a small movement $\varepsilon$ of the interface in a small step of time $\Delta t$, corresponding to an interface velocity of $V = \varepsilon/\Delta t$ (figure 1). In the area swept by the interface, $x = x^*(t)$, entropy is produced by the moving interface. The local equilibrium part of entropy increase is described by

$$\begin{aligned} -\Delta_{\Delta t}(TS_{\mathrm{eq}}) &= -\left[TS_{\mathrm{eq}}(t+\Delta t) - TS_{\mathrm{eq}}(t)\right] \\ &= \varepsilon\left[(1-C_S^*)(\mu_A^S - \mu_A^L) + C_S^*(\mu_B^S - \mu_B^L) - p\Delta v\right], \end{aligned} \tag{2.8}$$

where $\Delta v$ is the volume change and, for isobaric conditions, equation (2.8) is equivalent to the expression given in refs. [11,16]. In this occasion, all diffusion fluxes have vanished in the area swept by the interface, yielding a total entropy increase as

$$\begin{aligned} \Delta_{\Delta t}(TS_{\mathrm{ne}}) &= TS_{\mathrm{ne}}(t+\Delta t) - TS_{\mathrm{ne}}(t) \\ &= \int_{x^*(t_0)}^{x^*(t_0+\varepsilon)} [\alpha_D J_D^2(x,t_0) + v\alpha_0 (p^v)^2 + v\alpha_2 (P_{xx}^v)^2]\,\mathrm{d}x. \end{aligned} \tag{2.9}$$

The entropy production is evaluated by applying the differential quotient in the vanishing limit and applying the relation $V = \varepsilon/\Delta t$ by

$$\begin{aligned} -\frac{\mathrm{d}}{\mathrm{d}t}(TS)_{\mathrm{e}} &= -\lim_{\Delta t\to 0} \frac{TS_{\mathrm{e}}(t+\Delta t) - TS_{\mathrm{e}}(t)}{\Delta t} \\ &= \lim_{\Delta t\to 0} \frac{\varepsilon}{\Delta t}[(1-C_S^*)(\mu_A^S - \mu_A^L) + C_S^*(\mu_B^S - \mu_B^L) - p\Delta v] \\ &= V[(1-C_S^*)(\mu_A^S - \mu_A^L) + C_S^*(\mu_B^S - \mu_B^L) - p\Delta v]. \end{aligned} \tag{2.10}$$

With no change of volume, $\Delta v = 0$, equation (2.10) becomes identical to the classical result obtained in [11,16]. For the local non-equilibrium part, equation (2.9), we simplify the analysis by

neglecting the bulk pressure, i.e. $p^v \to 0$. Then, a Taylor series for the square flux and the square of the deviatoric part of the viscous pressure near the interface is introduced by

$$\left.\begin{aligned} J_D^2(x^*+\varepsilon,t_0) &= J_D^2(x^*,t_0)+\varepsilon\frac{\mathrm{d}}{\mathrm{d}x}J_D^2(x^*,t_0)+\cdots \\ \text{and}\qquad (P_{xx}^v)^2(x^*+\varepsilon,t_0) &= \left(P_{xx}^v\right)^2(x^*,t_0)+\varepsilon\frac{\mathrm{d}}{\mathrm{d}x}\left(P_{xx}^v\right)^2(x^*,t_0)+\cdots \end{aligned}\right\} \tag{2.11}$$

Using equation (2.11), the integral in (2.9) can be evaluated as

$$\begin{aligned} &\int_{x^*(t_0)}^{x^*(t_0+\varepsilon)}\left[\alpha_D J_D^2(x,t_0)+v\alpha_2\left(P_{xx}^v\right)^2\right]\mathrm{d}x \\ &\quad=\alpha_D\left[\varepsilon J_D^2(x^*,t_0)+\frac{\varepsilon^2}{2}\frac{\mathrm{d}}{\mathrm{d}x}J_D^2(x^*,t_0)+\cdots\right] \\ &\qquad+v\alpha_2\left[\varepsilon\left(P_{xx}^v\right)^2(x^*,t_0)+\frac{\varepsilon^2}{2}\frac{\mathrm{d}}{\mathrm{d}x}\left(P_{xx}^v\right)^2(x^*,t_0)+\cdots\right]. \end{aligned} \tag{2.12}$$

This leads to the following expression for the local non-equilibrium part in the entropy production

$$\begin{aligned} \frac{\mathrm{d}}{\mathrm{d}t}(TS)_{\mathrm{ne}} &= \lim_{\Delta t\to 0}\frac{TS_{\mathrm{ne}}(t+\Delta t)-TS_{\mathrm{ne}}(t)}{\Delta t} \\ &=\alpha_D\lim_{\Delta t\to 0}\left[\frac{\varepsilon}{\Delta t}J_D^2(x^*,t_0)+\frac{\varepsilon^2}{2\Delta t}\frac{\mathrm{d}}{\mathrm{d}x}J_D^2(x^*,t_0)+\cdots\right] \\ &\quad+v\alpha_2\lim_{\Delta t\to 0}\left[\frac{\varepsilon}{\Delta t}\left(P_{xx}^v\right)^2(x^*,t_0)+\frac{\varepsilon^2}{2\Delta t}\frac{\mathrm{d}}{\mathrm{d}x}\left(P_{xx}^v\right)^2(x^*,t_0)+\cdots\right] \\ &=\alpha_D V J_D^2(x^*,t_0)+\alpha_D\left[\lim_{\Delta t\to 0}\Delta t V^2\frac{\mathrm{d}}{\mathrm{d}x}J_D^2(x^*,t_0)+\cdots\right] \\ &\quad+v\alpha_2 V\left(P_{xx}^v\right)^2(x^*,t_0)+v\alpha_2\left[\lim_{\Delta t\to 0}\Delta t V^2\frac{\mathrm{d}}{\mathrm{d}x}\left(P_{xx}^v\right)^2(x^*,t_0)+\cdots\right] \\ &\approx\alpha_D V J_D^2(x^*,t_0)+v\alpha_2 V\left(P_{xx}^v\right)^2(x^*,t_0), \end{aligned} \tag{2.13}$$

where $P_{xx}^v(x^*,t_0)$ is the deviator of the viscous pressure at the interface and $J_D(x^*,t_0)$ is the diffusion flux away from the interface. Note that this flux generally does not vanish (except in the special case of diffusionless solidification in which $C_L^*=C_S^*$), leading to the local non-equilibrium contribution for interface velocities $V$ smaller than the solute diffusion speed $V_D$ in bulk liquid, i.e. with $V<V_D$, where $V_D\equiv V_D^{(B)}$ is the maximum speed for the diffusion of $B$-atoms.

Finally, using equations (2.10) and (2.13), the total entropy production per unit time at the interface is given by

$$\begin{aligned} -\frac{\mathrm{d}(TS)_{\mathrm{Interface}}}{\mathrm{d}t} &= V\cdot\left[(1-C_S^*)(\mu_A^S-\mu_A^L)+C_S^*(\mu_B^S-\mu_B^L)+\alpha_D J_D^2(x^*,t_0)\right] \\ &\quad-V\cdot[p\Delta v-v\alpha_2(P_{xx}^v)^2(x^*,t_0)]. \end{aligned} \tag{2.14}$$

## (c) Gibbs free energy change on rapid solidification

Using the established system of thermodynamic relations [14,16,17], one obtains

$$\left.\begin{aligned} -\frac{\mathrm{d}(TS)_{\mathrm{Interface}}}{\mathrm{d}t} &= \frac{\mathrm{d}G}{\mathrm{d}t}=-v_m^{-1}V\Delta G \\ \text{and}\qquad \frac{\mathrm{d}G}{\mathrm{d}t} &= J_D X_D+J_C X_C+J_P X_P, \end{aligned}\right\} \tag{2.15}$$

where $G$ and $\Delta G$ are the Gibbs free energy and the Gibbs free energy change on solidification, respectively. Taking into account that the change in Gibbs free energy $\Delta G$ proceeds at a constant

volume, i.e. at $\Delta v = 0$, then, as follows from equation (2.14), the diffusion flux $J_D$ and the crystallization flux $J_C$ together with their conjugate driving forces, $X_D$ and $X_C$, respectively, are defined in equation (2.15) by

$$\left.\begin{aligned} &J_D = -v_m^{-1} V (C_L^* - C_S^*), \quad X_D = \Delta\mu_A - \Delta\mu_B + \alpha_D (C_L^* - C_S^*) V^2, \\ &J_C = -v_m^{-1} V, \quad X_C = (1 - C_L^*)\Delta\mu_A + C_L^* \Delta\mu_B \\ \text{and} \quad &J_P = -v_m^{-1} V, \quad X_P = v\alpha_2 (P_{xx}^v)^2, \end{aligned}\right\} \tag{2.16}$$

where $\Delta\mu_A = \mu_A^S - \mu_A^L$ and $\Delta\mu_B = \mu_B^S - \mu_B^L$ are the differences in the chemical potentials for $A$- and $B$-atoms, respectively. In the linear approximation, $J_D \propto X_D$, $J_C \propto X_C$ and $J_P \propto X_P$ one can obtain the following relations between fluxes and conjugate driving forces:

$$\left.\begin{aligned} &(C_L^* - C_S^*)\frac{V}{v_m} = L_D \left[\Delta\mu_A - \Delta\mu_B + \alpha_D (C_L^* - C_S^*) V^2\right], \\ &\frac{V}{v_m} = L_C \left[(1 - C_L^*)\Delta\mu_A + C_L^* \Delta\mu_B\right] \\ \text{and} \quad &\frac{V}{v_m} = L_P v\alpha_2 \left(P_{xx}^v\right)^2, \end{aligned}\right\} \tag{2.17}$$

where $L_D$, $L_C$ and $L_P$ are the kinetic coefficients for diffusion and crystal growth due to the driving force for atom attachment and due to the elastic and plastic relaxation, respectively. Several limiting cases can be outlined from equation (2.17). *First*, for the diffusionless (chemically partitionless) solidification, the analytical solution [33] gives naturally $C_L^* = C_S^*$ at $V \geq V_D$. Then, the first equation gives the expression $\Delta\mu_A = \Delta\mu_B$, which indicates the equality of the chemical potential differences for rapid diffisionless solidification. From this follows the *second* case, which describes the growth kinetics as for a pure one-component substance upon the diffusionless solidification given by the second equation from equation (2.17): $V = v_m L_C \Delta\mu_A$ with $V \geq V_D$. The *third* equation of equation (2.17) predicts that the viscous relaxation of stresses may cause the motion of the solid/liquid interface.

Using the relations from equation (2.16) in equation (2.15), one obtains

$$\Delta G = (1 - C_S^*)\Delta\mu_A + C_S^* \Delta\mu_B + \alpha_D (C_L^* - C_S^*)^2 V^2 + v\alpha_2 (P_{xx}^v)^2. \tag{2.18}$$

This expression represents the Gibbs free energy change at the solid/liquid interface and describes the driving force for interface motion. Neglecting relaxation of the diffusion flux $\alpha_D = 0$, and relaxation of viscous stresses $\alpha_2 = 0$, equation (2.18) takes its standard form given and analysed in refs. [11,13,14,16]. The additionally included effects in equation (2.18), which may accompany rapid solidification, give the following contribution to $\Delta G$ (see also refs. [34,35]): the diffusion flux relaxation $\propto V^2$, and the viscous stress relaxation $\propto (P_{xx}^v)^2$ should increase the driving force for interface motion.

The established thermodynamic relation for chemical diffusion in rapid solidification (2.18) introduces a pressure term, $\propto (P_{xx}^v)^2$, that may have the potential to advance the current understanding of non-equilibrium solidification. More specifically, it may bring about:

- new insights into undercooled solidification under hydrostatic pressures or in centrifugal casting [36];
- the analysis of dendrite growth on the inner core of Earth [37];
- influence of (elastic and plastic) stresses and dislocation motion on crystal growth kinetics [38].

The quantitative effect of the pressure term $\propto (P_{xx}^v)^2$ on solidification will be clarified in the future works.

Finally, one should note that a thermodynamic analysis was used to describe the liquidus slope in kinetic phase diagram with the appropriate methods described in detail in refs. [12,13,15,17].

Using these methods and neglecting the viscous stresses, $P^v_{xx} = 0$, one can, in particular, find from the driving force, equation (2.18), the velocity-dependent liquidus slope, $m_v(V)$, as [34,35]

$$m_v = \begin{cases} \dfrac{m_e}{1-k_e}\left\{1 - k_v + \ln\left(\dfrac{k_v}{k_e}\right) + (1-k_v)^2\dfrac{V^2}{V_D^2}\right\}, & V < V_D, \\ \dfrac{m_e \ln k_e}{k_e - 1} \equiv \text{const}, & V \geq V_D, \end{cases} \tag{2.19}$$

where $m_e$ and $k_e$ are the equilibrium liquidus slope and solute partition coefficient (which can be obtained from the phase diagram or calculated using CALPHAD), respectively, and $k_v \equiv C^*_S/C^*_L$ is the velocity-dependent partition coefficient. The function (2.19) differs slightly from the one derived for the approximation of dilute mixtures [17]. For finite concentrations, the liquidus slope, equation (2.19), depends on the square of the interface velocity, $m_v \propto (V/V_D)^2$, explicitly.[1] In the theory of diluted mixtures/alloys, the kinetic liquidus was obtained as linearly proportional to the velocity [17], i.e. $m_v \propto V/V_D$. However, as we show in the following section, the predictions of the crystal growth kinetics are quantitatively valid using equation (2.19) and ref. [17] due to the fact that the strongest dependence of $m_v$ on $V$ is dictated by the nonlinear behaviour of the atomic distribution function at the interface $k_v(V)$. An estimation of the pressure influence (with $P^v_{xx} \neq 0$) on the velocity-dependent kinetic liquidus should be specially given. On the one hand, the pressure plays an insignificant role in the crystal growth under usual circumstances (see Chapter 2 in the monograph of Glicksman [39]). On the other hand, the growth of dendrites might be essentially influenced on the inner core of the Earth from the magma's side [37], where the pressure and temperature are important parameters for dynamical equilibrium at the solid/liquid interface. How important the effect of viscous pressure relaxation on the rapidly moving solid/liquid interface is should be clarified in forthcoming works.

## 3. Dendrite growth model

In the following, we consider two models for rapid dendritic growth. The first model was formulated to describe primary growth developed for dendrites of interstitial and substitutional solutions. The model was tested in numerous cases of binary and ternary alloys solidifying from undercooled melts [19–23]. We formulate this model for two reasons. First, we compare kinetic curves for two cases of liquidus line slopes as formulated in §2 and as derived in [17]. The second model appears as an extended advanced first model to describe kinetic curves in glass-forming alloys exhibiting a maximum in the dendrite growth velocity/melt undercooling relationship.

### (a) Undercooling balance and stability criterion

Equations of a sharp interface model were formulated for the analysis of rapid solidification taking into account deviations from equilibrium at the solid/liquid interface and in bulk liquid [19,20,33,40,41]. At the solid/liquid interface, a deviation from local thermodynamic equilibrium may arise due to atom attachment kinetics and solute trapping. A deviation from thermodynamic equilibrium in the liquid may exist in the diffusion field of solutes, which has no time to relax to local chemical equilibrium due to the rapidly growing dendrite. This model combines a selection criterion for stable dendritic growth mode and the balance of different undercooling contributions at the dendritic tip.

[1]In its implicit form, the kinetic liquidus (2.19) depends also on the velocity-dependent function $k_v(V)$, which is the solute partition coefficient, the coefficient of chemical segregation or, in other words, the atoms distribution coefficient at the interface, see also [10,12,13,15,17].

The total undercooling, $\Delta T = T_m + m_e C_0 - T_0$, represents the undercooling balance at the dendrite tip as

$$\Delta T = \Delta T_T + \Delta T_C + \Delta T_N + \Delta T_R + \Delta T_K, \tag{3.1}$$

where $T_m$ is the melting temperature of the solvent, $C_0$ and $T_0$ are the initial (i.e. nominal or far-field) composition and temperature of the liquid, respectively. The balance includes the thermal undercooling $\Delta T_T$

$$\Delta T_T = T_Q \mathrm{Iv}(P_T), \tag{3.2}$$

the undercooling $\Delta T_C$ due to solute redistribution at the solid–liquid interface

$$\Delta T_C = \begin{cases} k_v \Delta_v \dfrac{\mathrm{Iv}(P_C)}{1-(1-k_v)\mathrm{Iv}(P_C)}, & V < V_D, \\ 0, & V \geq V_D, \end{cases} \tag{3.3}$$

with the Ivantsov functions $\mathrm{Iv}_{T(C)}(P_{T(C)})$ defined by

$$\mathrm{Iv}_{T(C)}(P_{T(C)}) = \begin{cases} \mathrm{P_{T(C)}} \exp(\mathrm{P_{T(C)}}) E_1(\mathrm{P_{T(C)}}), & \text{in the 3D space,} \\ \sqrt{\pi \mathrm{P_{T(C)}}} \exp(\mathrm{P_{T(C)}}) \mathrm{erfc}\sqrt{P_{T(C)}}, & \text{in the 2D space,} \end{cases} \tag{3.4}$$

exponential integral function $E_1(\mathrm{P_{T(C)}})$ of the first kind and the thermal/chemical Peclét numbers $P_{T(C)}$,

$$E_1(P_{T(C)}) \equiv \int_{P_{T(C)}}^{\infty} \frac{\exp(-u)}{u}\,\mathrm{d}u, \quad P_T = \frac{VR}{D_T}, \quad P_C = \frac{VR}{D_L}, \tag{3.5}$$

where $T_Q = \Delta H_f / c_p$ is the adiabatic temperature of solidification (hypercooling), $\Delta H_f$ is the enthalpy of melting, $c_p$ is the heat capacity, $D_T$ and $D_L$ are the thermal and chemical diffusion coefficients, respectively, and $V$ is the velocity of the dendrite tip with radius $R$.

The velocity-dependent non-equilibrium interval $\Delta_v$ of solidification in equation (3.3) is given by

$$\Delta_v = \begin{cases} \dfrac{m_v C_0 (1-k_v)}{k_v}, & V < V_D, \\ 0, & V \geq V_D. \end{cases} \tag{3.6}$$

Note that if the dendrite tip velocity $V$ is equal to or greater than the solute diffusion speed $V_D$, the constitutional undercooling $\Delta T_C$ is equal to zero, corresponding to the transition to the diffusionless regime of solidification.

Finally, the undercooling $\Delta T_N$ arising due to the shift of the equilibrium liquidus line from its equilibrium position in the kinetic phase diagram of steady-state solidification is given by

$$\Delta T_N = (m_e - m_v) C_0. \tag{3.7}$$

The curvature undercooling $\Delta T_R$ due to the Gibbs–Thomson effect and the kinetic undercooling $\Delta T_K$ that change the driving force for interface movement due to the atomic attachment from the liquid to the solid phase are defined as

$$\Delta T_R = \frac{2 d_0 T_Q}{R} \quad \text{and} \quad \Delta T_K = \frac{V}{\mu_k}, \tag{3.8}$$

where $d_0$ is the capillary length and $\mu_k$ is the interface kinetic coefficient.

The velocity-dependent liquidus slope is described by [17]

$$m_v = \begin{cases} \dfrac{m_e}{1-k_e}\left\{1-k_v+\ln\left(\dfrac{k_v}{k_e}\right)+(1-k_v)^2\dfrac{V}{V_D}\right\}, & V<V_D, \\ \dfrac{m_e \ln k_e}{k_e-1}\equiv \text{const.}, & V\geq V_D, \end{cases} \tag{3.9}$$

and the velocity-dependent partition coefficient $k_v \equiv C_S^*/C_L^*$ is given by [33]

$$k_v = \begin{cases} \dfrac{(1-V^2/V_D^2)k_e+V/V_{DI}}{(1-V^2/V_D^2)[1-(1-k_e)C_L^*]+V/V_{DI}}, & V<V_D, \\ 1, & V\geq V_D, \end{cases} \tag{3.10}$$

where $C_S^*$ and $C_L^*$ are solute concentrations of the solid and liquid at the dendrite tip, respectively, with

$$C_L^*(P_C) = \begin{cases} \dfrac{C_0}{1-(1-k_v)\mathrm{Iv}_C(P_C)}, & V<V_D, \\ C_0, & V\geq V_D, \end{cases} \tag{3.11}$$

Here $m_e$ is the slope of the liquidus line in the phase diagram of coexisting phases, and $k_e$ is the equilibrium partitioning coefficient of solute atoms.

Because equation (3.1) is the only equation for two variables, $V$ and $R$, at the given (and experimentally measurable) undercooling $\Delta T$, a second equation is required to close the problem, and it is given by the stability condition [41]

$$R = \begin{cases} \dfrac{1}{\sigma^*}\cdot\dfrac{d_0\Delta_0}{T_Q P_T \xi_T - 2\Delta_v P_C \xi_C}, & V<V_D, \\ \dfrac{1}{\sigma^*}\cdot\dfrac{d_0\Delta_0}{T_Q P_T \xi_T}, & V\geq V_D, \end{cases} \tag{3.12}$$

with $\Delta_0$ the temperature interval of solidification in the phase state defined by

$$\Delta_0 = \begin{cases} \dfrac{m_e(k_e-1)C_0}{k_e}, & \text{for alloys,} \\ T_Q, & \text{for pure substance, } C_0 = 0. \end{cases} \tag{3.13}$$

Condition (3.12) defines the dendrite tip growing in the stable mode due to the anisotropy $\varepsilon_c$ of the interfacial energy and the stability parameter $\sigma^* \propto \varepsilon_c^{7/4}$ [42–45]. The thermal stability function for rapid solidification is given by

$$\xi_T(P_T) = \left[1+a_1\sqrt{\alpha_d}P_T\left(1+\frac{a_0 D_T \beta_0}{d_0}\right)\right]^{-2}, \tag{3.14}$$

where $a_0$ and $a_1$ are the asymptotic coefficients of sewing the large thermal Peclét numbers regime and growth kinetics regime, respectively, $\beta_0 = 1/(\mu_k T_Q)$ is the kinetic parameter of growth and $\alpha_d = 15\varepsilon_c$ is the stiffness. The chemical stability function for rapid solidification is described by

$$\xi_C(P_C, W) = \begin{cases} \left[1+a_2\sqrt{\alpha_d}P_C^*\left(1+\dfrac{a_0 D_L \beta_0}{d_{0\mathrm{CD}}}\right)\right]^{-2}, & V<V_D, \\ 0, & V\geq V_D, \end{cases} \tag{3.15}$$

where $a_2$ is the asymptotic coefficients of sewing the large thermal Peclét numbers regime, $d_{0\mathrm{CD}}$ is the chemical capillary length and $P_C^* = P_C/\sqrt{1-V^2/V_D^2}$. With the local equilibrium limit, $V_D \to \infty$, the stability growth mode by equations (3.12)–(3.15) describes the regime of Fickean diffusion taken into account by Trivedi & Kurz [46] for rapid dendritic growth [47]. Within the limit of small Peclét numbers, $P_T \ll 1$ and $P_C^* \ll 1$, and with the local equilibrium limits $V_{DI} \to \infty$ and $V_D \to \infty$, equations (3.12)–(3.15) transform to the previously obtained conditions of Ben Amar and Pelce [43]. The selection criteria (3.12)–(3.15) are written for a fourfold symmetry of the crystal lattices. It can be generalized to other crystalline symmetries [48,49].

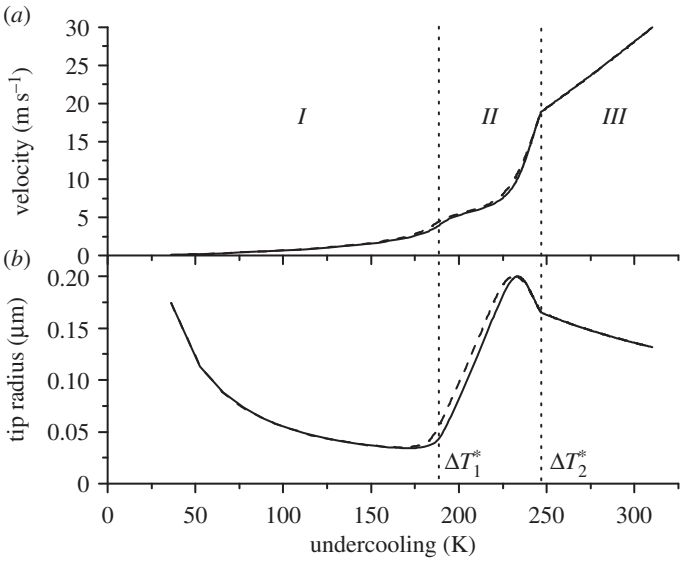


**Figure 2.** Predictions of the model given by two main equations (3.1) and (3.12). Calculations were made using the parameters for Ni–0.7 at.%B taken from ref. [41] for a dendrite velocity $V$ (*a*) and a tip radius $R$ (*b*). Different growth regimes are separated from each other by the critical undercoolings, $\Delta T_1^*$ and $\Delta T_2^*$ such that the solute diffusion limited growth of dendrites proceeds for $\Delta T < \Delta T_1^*$ (range *I*), the intermediate stage consisting of solute diffusion limited and thermally controlled growth exists in the range $\Delta T_1^* < \Delta T < \Delta T_2^*$ (range *II*), and purely thermally controlled dendritic solidification occurs at $\Delta T > \Delta T_2^*$ (range *III*). The solid line was obtained for the kinetic liquidus slope given by equation (3.9) and the dashed line was calculated using the kinetic liquidus slope given by equation (2.19). The difference between both curves (dashed and solid) are nearly negligible and they are both consistent with experimental data in a whole range of measurable undercoolings and dendrite velocities within the error bars of experiment, see [41].

## (b) Predictions of the model: dendrite velocity and tip radius

The model equations (3.1)–(3.15) describe (i) solute diffusion limited growth of dendrites (i.e. growth of 'solutal' dendrites at low undercoolings), (ii) solute diffusion limited and thermally controlled growth of dendrites (i.e. growth of solutal and thermal dendrites in the intermediate range of undercoolings), and (iii) purely thermally controlled dendritic solidification at high undercoolings. These regimes are shown in figure 2 and were previously described for alloy dendrites (see [22,41,50] and references therein).

The transition from solute diffusion limited growth to the thermally controlled regime of growth in the range $\Delta T_1^* < \Delta T < \Delta T_2^*$ is characterized by the change from slow growth at $\Delta T < \Delta T_1^*$ to the increase of the interface velocity, figure 2*a*, and increase of the dendrite tip radius up to its maximal value followed by a decrease at further increasing velocities (figure 2*b*). Such nonlinear behaviour in $V$ and $R$ exists due to the change in the characteristic spatial lengths defining the dendrite velocity and tip radius, particularly the solute diffusion length and the thermal diffusion length.

At the critical undercooling, $\Delta T = \Delta T_2^*$, the velocity $V = V_D$ leads to complete solute trapping, $C_L^* = C_S^* = C_0$, for the dendrite stems [51]. Beyond this critical point, dendrite growth occurs without solute redistribution and with the initial chemical composition, i.e. in the diffusionless (chemically partitionless) regime. Thus, in the range $\Delta T \geq \Delta T_2^*$, the dendrite growth is thermally controlled only. This result has a clear physical meaning: a source of concentrational disturbances at the solid/liquid interface moving at a velocity equal to or higher than the maximum speed of these disturbances cannot disturb the liquid phase ahead of itself. Therefore, when the interface velocity $V$ passes through the critical point $V = V_D$, the solidification mechanism changes qualitatively and the undercooling in liquid will not depend on the solute distribution during

diffusionless growth. In a microscopic interpretation, the atoms have no time for diffusion jumps if $V \geq V_D$; they are all stochastically attaching to the interface and instantaneously captured by the solid phase.

Finally note that the transition to diffusionless solidification proceeds sharply at $V = V_D$ and $\Delta T = \Delta T_2^*$ with a steep change of slope of the 'velocity versus undercooling' and 'tip radius versus undercooling' curves (figure 2). Such sharp transition in the growth kinetics at some critical value of non-equilibrium governing parameter (undercooling, supersaturation) is related to the 'kinetic phase transitions', as defined by Alexander Chernov [52], that was observed in experiments on rapid solidification [7,8,22] and analysed using different models (see ref. [25] and references therein).

## 4. Dendritic solidification in glass-forming metals and alloys

### (a) Model equations

The curves shown in figure 2*a* exhibit a monotonic increase of the dendrite tip velocity with the undercooling that is typically observed in experiments on solidifying interstitial and substitutional alloys [7,8,13]. However, there is a wide class of alloys exhibiting a maximum of the dendrite velocity that is situated between liquidus temperature and glass temperature (at which an amorphous phase forms and the building of primary crystalline structures is impossible) [26, 28]. This class includes glass-forming alloys and, quite frequently, congruently melting alloys. To describe such behaviour, the model of dendritic solidification in equations (3.1)–(3.15) can be reformulated and extended to describe the kinetic curves in glass-forming alloys.

Consider the solidification of a glass-forming alloy which is congruently melting without chemical segregation. In this case, the system of equations (3.1)–(3.15) is reduced to the balance of undercoolings as

$$\Delta T = \Delta T_T + \Delta T_R + \Delta T_K, \tag{4.1}$$

with the thermal, capillary/curvature and kinetic contributions

$$\Delta T_T = T_Q \mathrm{Iv}(P_T), \quad \Delta T_R = \frac{2d_0 T_Q}{R}, \quad \Delta T_K = \frac{V}{\mu_k(\Delta T)}, \tag{4.2}$$

where the kinetic coefficient $\mu_k(\Delta T)$ is a strongly dependent function of undercooling $\Delta T$. The stable growth mode of the dendrite tip is defined from equations (3.12)–(3.15) as

$$\left.\begin{aligned} R &= \frac{1}{\sigma^*} \cdot \frac{d_0 \Delta_0}{T_Q P_T \xi_T}, \quad \sigma^* = \sigma_0 \varepsilon_c^{7/4} \\ \text{and} \quad \xi_T &= \left[1 + a_1 \sqrt{\alpha_d} P_T \left(1 + \frac{a_0 D_T \beta_0}{d_0}\right)\right]^{-2}. \end{aligned}\right\} \tag{4.3}$$

All the coefficients and functions of equations (4.1)–(4.3) are defined in §3.

### (b) Kinetic undercooling

The crystal growth models based on the rate kinetic theory give excellent predictions of the molecular dynamics simulation data at small undercoolings (see appendix A, figure 5*a*). With the increasing undercooling, the crystal growth velocity exhibits clear nonlinearity which may not be predicted by the models based on the rate kinetic theory (see appendix A, figure 5*b*).

So far, the nonlinearity in the velocity versus undercooling relationships has been obtained similarly to curves with saturation, which are limited by the maximum velocity of the phase field (see [53] as well as the solid curve with saturation in figure 5*b*). To predict the nonlinear curves with the velocity maximum [54–56] exhibiting one of the distinct characteristics of the crystallization of glass-forming metals and alloys [26,28], we use the travelling wave solution (B 17) of the kinetic phase field model for obtaining the dependence of the kinetic undercooling on the interface velocity.

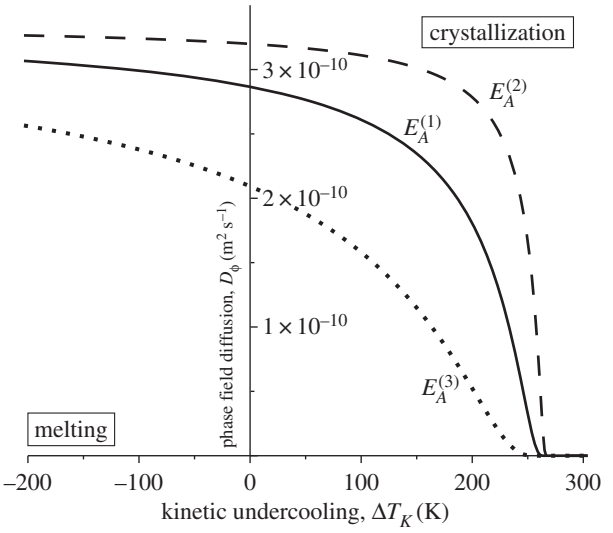


**Figure 3.** Phase field diffusion coefficient versus kinetic undercooling. Curve $E_A^{(1)}$ corresponds to $E_A = 42.11$ K, fitted to the experimental data on crystallization of a $Cu_{50}Zr_{50}$ alloy (figure 4). Curve $E_A^{(2)}$ corresponds to higher $E_A = 126.34$ K; $E_A^{(3)}$ corresponds to $E_A = 12.63$ K. The coefficients $D_\phi^0 = 3.35 \times 10^{-10}$ (m$^2$ s$^{-1}$) and $T_A = 940$ K are the same for all calculations.

Using the approximations $\Delta G \ll k_B T$ and the simplest possible expression for the driving force [57]

$$\Delta G = \frac{\Delta H_f(-\Delta T_K)}{T_m}, \quad \Delta T_K = T_m - T, \tag{4.4}$$

equation (B 17) takes the form (see appendix B)

$$V = \beta_K^{(\mathrm{PFM})} \Delta T_K, \tag{4.5}$$

which is consistent with the approximations of the kinetic equations (A 4) and (A 5) and for which the kinetic coefficient of growth depends on the kinetic undercooling $\Delta T_K$ as

$$\beta_K^{(\mathrm{PFM})} = \frac{D_\phi(\Delta T_K)\Delta H_f}{\gamma T_m \sqrt{1 + \left[(D_\phi(\Delta T_K)\Delta H_f/\gamma T_m V_\phi(\Delta T_K))\Delta T_K\right]^2}}. \tag{4.6}$$

The maximum propagation speed of the phase field depends on the undercooling through the diffusion of the phase field as

$$V_\phi(\Delta T_K) = \sqrt{\frac{D_\phi(\Delta T_K)}{\tau_\phi}}, \tag{4.7}$$

where $\tau_\phi$ is the relaxation time of the gradient flow, $\partial\phi/\partial t$, of the phase field (which is taken in the present analysis as a constant, independent of temperature). The diffusion coefficient of the phase field is taken in the form

$$D_\phi(\Delta T_K) = D_\phi^0 \exp\left(-\frac{E_A}{T_m - \Delta T_K - T_A}\right), \tag{4.8}$$

where the diffusion factor $D_\phi^0$, the temperature $T_A$ and the energetic barrier $E_A$ are the parameters of the phase field propagation. Particularly, $T_A$ controls the temperature at which a drastic change in the crystal growth kinetics may occur.

Figure 3 shows the dependence of the phase field diffusion coefficient, equation (4.8), on the undercooling ($\Delta T_K > 0$) and the superheating ($\Delta T_K < 0$). As the figure shows, the change in the barrier $E_A$ can lead to a qualitative change in the behaviour of the phase field diffusion. The higher

value of $E_A$ (see the curve the curve $E_A^{(2)}$) gives a gradual change of the phase field diffusion around the equilibrium melting point and a steep decrease of the phase field diffusion at larger undercoolings far from the melting point. By contrast, for the smaller value of $E_A$ the curve $E_A^{(3)}$ exhibits a linear change of the phase field diffusion with the change of $\Delta T_K$ up to its zero value, $D_\phi = 0$.

One has to finally note that the form of the diffusion coefficient, equation (4.8), is similar to the form of the phase field mobility $M_\phi(T)$ given by Novokreshchenova & Lebedev [58]. This form is inversely proportional to the kinematic viscosity described by the Vogel–Fulcher–Tamman expression [59] which predicts a strongly anomalous increasing viscosity as the temperature begins to approach the glass temperature. Function (4.8) shows inverse behaviour: as soon as the undercooling approaches its critical value, the phase field diffusion begins its steep decrease down to its zero value exactly at the critical undercooling.

## (c) Kinetics of dendritic growth in $Cu_{50}Zr_{50}$

$Cu_{50}Zr_{50}$ is a glass-forming alloy which has been investigated in detail by heating, melting, cooling and solidifying droplets processed in an electrostatic levitation facility [27,60]. The dendrite growth velocity was measured for undercoolings of up to $\Delta T = 311$ K. It was found that the velocity first increases and then decreases as the total undercooling increases. The congruently melting $Cu_{50}Zr_{50}$ alloy solidifies without chemical segregation and, together with the first measurements on Ag [61], it was the metallic system for which the transition from thermodynamically to kinetically controlled growth was firstly experimentally observed [27].

Wang *et al.* [29] suggested a model of dendritic growth in which the kinetic undercooling was defined via a dendrite growth coefficient that is dependent on the viscosity behaviour. They tried to describe the experiments of ref. [27] in the whole range of undercoolings $\Delta T(\mathrm{K}) \leq 311$. The dash-dotted line in figure 4 shows that the experimental data are well described up to an undercooling of approximately $\Delta T = 290$K. The interval $290 < \Delta T\ (\mathrm{K}) \leq 311$ shows a drastic decrease of the velocity with its a further abrupt drop at the critical undercooling $\Delta T = 311$K that is not described by the smooth and gradually changing $V(\Delta T)$-curve of Wang et al. (figure 4). The same abrupt behaviour has also been obtained for the solidification of Cu–Zr-based alloys, particularly $Zr_{50}Cu_{30}Ni_{20}$ and $Zr_{50}Cu_{45}Ni_5$ alloys [62]. Therefore, the model presented here, equations (4.1)–(4.8), has been applied to describe the experimental data on Cu–Zr-based alloys exhibiting a maximum of a velocity and an abrupt drop behaviour at the highest critical undercooling.

Using the material parameters of the $Cu_{50}Zr_{50}$ alloy from table 1, the dendrite growth velocity was calculated by the model, equations (4.1)–(4.8). Note, to obtain parameters for the phase field diffusion and relaxation time, we supposed that a part of the velocity versus undercooling curve is described mainly by the kinetic undercooling $\Delta T_K$. Therefore, just to obtain optimal fitting for $\tau_\phi$, $D_\phi^0$, $E_A$ and $T_A$ we have used the 'kinetic undercooling shift', $\Delta T_k^\Delta = 70$ (K), which is a shift of the curve $V - \Delta T$ from the origin along the $\Delta T$-axis.

Figure 4 shows the comparison of the present model with the predictions of Wang *et al.* and experimental data obtained from samples processed by an electromagnetic levitator on the Ground [27,63] and under microgravity generated during parabolic flights [60,62]. It can be seen that the solid line calculated by the full model (4.1)–(4.8) describes the whole set of experimental data including the abrupt drop in the velocity at the critical undercooling $\Delta T \approx 311$ K. If we exclude the local non-equilibrium effect of the relaxation of the gradient flow, i.e. $\tau_\phi \to 0$ and $V_\phi \to \infty$ in equations (4.7) and (4.8), the square root will yield unity in equation (4.5) and we get the velocity as plotted by the dotted line in figure 4. More specifically, it is shown in the insert of figure 4 how the predicted velocity lies far from the experimental data if the local non-equilibrium effect in the phase field dynamics is not taken into account.

The necessity to introduce the gradient flow of the phase field as an additional thermodynamic variable (see appendix B) lies in the fact that with the increase of undercooling in glass-forming alloy one can find a transition from single atoms and single clusters to chains of connected clusters (see data of molecular dynamics simulations in [64]). Such chains represent long molecules

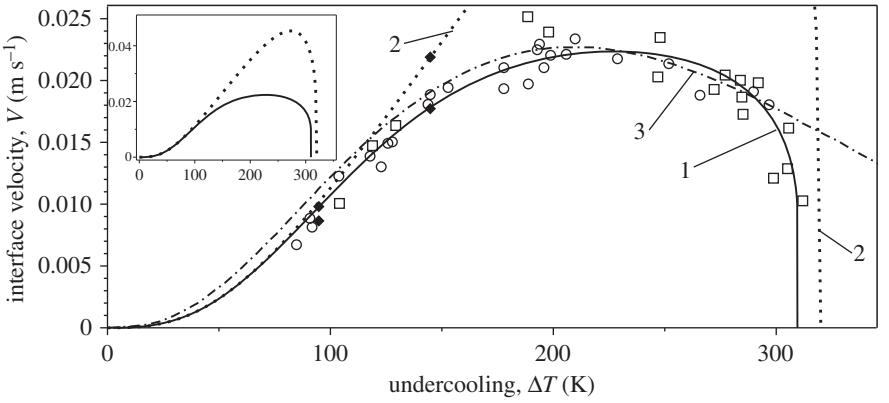


**Figure 4.** Experimental data on the dendrite growth velocity of $Cu_{50}Zr_{50}$ measured by Q. Wang *et al.* (open squares, [27]), R. Kobold *et al.* (open circles, [63]) and P. Paul (solid diamonds, [60]). The theoretical curves display: (1) solid curve, complete model (4.1)–(4.8); (2) dotted curve, model (4.1)–(4.8) with instant relaxation of the gradient flow, $\tau_\phi = 0$; (3) dash-dotted curve, model of Wang *et al.* [29]. The insert shows how the theoretical prediction may lie far from experimental data if the gradient flow is not included in the model as an additional thermodynamic variable (see appendix B).

**Table 1.** Material parameters of the $Cu_{50}Zr_{50}$ alloy used in the present calculations.

| parameter | value | source |
|---|---|---|
| $T_m$ (K), melting temperature | 1208 | [27] |
| $\Delta H_f$ (J kg$^{-1}$), enthalpy of fusion | $8.78 \times 10^8$ | [27] |
| $T_Q$ (K), adiabatic temperature | 204.87 | [27] |
| $d_0$ (m), capillary length | $6.83 \times 10^{-10}$ | [27] |
| $\gamma$ (J m$^{-2}$), interface energy | 0.6 | [27] |
| $\varepsilon_c$ (–), anisotropy of interface energy | 0.15 | present work |
| $\sigma_0$ (–), constant of selection criterion | $12.8 \times 10^{-4}$ | present work |
| $\tau_\phi$ (s), relaxation time | $3.41 \times 10^{-7}$ | present work |
| $D^0_\phi$ (m$^2$ s$^{-1}$), diffusion factor | $3.35 \times 10^{-10}$ | present work |
| $E_A$ (K), energetic barrier | 42.11 | present work |
| $T_A$ (K), pseudo-glass temperature | 940 | present work |

which lead to a delay in the kinetic processes in the bulk of the liquid phase and at the solid/liquid interface. In the present model, this transition is phenomenologically expressed by the special form of the phase field diffusion coefficient (4.8) which describes the delay in the phase field propagation up to an interface velocity of zero. The critical undercooling at which one may obtain this interface velocity characterizes the impossibility of the phase field propagating due to the specific structure of the undercooled liquid represented by the very long chains of connected clusters. Behind this critical undercooling the remaining liquid may transform into the amorphous phase (see ref. [60] and references therein). Therefore, glass forms at undercoolings larger than the critical undercooling for the zero velocity of the solid/liquid interface. Details and numerical values for these critical undercoolings can be clarified in an atomistic and phenomenological investigation of crystallization and amorphization processes.

Finally, even though we describe experimental data on solidification kinetics of the $Cu_{50}Zr_{50}$ melt quite well, figure 4, a couple of important issues should be noted as well. *First*, the primary phase which may solidify from the undercooled $Cu_{50}Zr_{50}$ melt is the intermetallic phase of

*B*2-type. Solidification of intermetallic compounds may be drastically influenced by the order–disorder transition at the rapidly moving interface [65–69], therefore, this effect leading to pronounced disorder trapping should be introduced into the model of the $Cu_{50}Zr_{50}$ solidification. *Second*, intensive investigations of the liquid structure [70,71] and crystallizing phase [72] by *in-situ* high-energy synchrotron X-ray diffraction on electrostatically levitated samples show that $Cu_{50}Zr_{50}$ always solidifies as the *B*2-phase over the whole accessible undercooling range up to 310K. However, periodicity of such measurements was about 5 s [72], which might overcome the duration of decomposition of a primary metastable phase. Indeed, the primary crystalline phase can appear as a new metastable phase at high undercooling with its lifetime smaller than the second phase [62]. Therefore, phase selection and sequence of phase precipitation may also affect the solidification kinetics, which has to be considered as a further advancement of theoretical models for dendrite growth in glass-forming melts.

## 5. Conclusion

The thermodynamic driving force for rapid solidification that takes into account both the difference in chemical potential and the relaxation of stresses has been derived and analysed. The model for rapid dendritic growth including the transition to diffusionless solidification has been tested and quantified. In particular, we compared the influence of the kinetic liquidus derived for the binary diluted and concentrated mixtures on the growth kinetics of alloy dendrites. On the basis of this model, the description of dendritic solidification in glass-forming alloys of alloy systems with congruent melting phases is possible. The solidification kinetics of this class of alloys is well described by the theory which includes local non-equilibrium effects in the form of relaxation of the gradient flow in the phase field. Good comparison with experimental data confirms the initial theoretical assumption about the predominant influence of local non-equilibrium effects in solidification under large driving forces.

Data accessibility. This article has no additional data.

Authors' contributions. All authors contributed equally to the present review paper.

Competing interests. The authors declare that they have no competing interests.

Funding. This work was supported by the Russian Science Foundation (grant no. 16-11-10095) and the German Space Center Space Management under contract no. 50WM1541.

## Appendix A. Models based on the rate kinetic theory

The rate kinetic theory (or thermally activated growth theory [73]) in application to melting/crystallization compares two atomic fluxes at the moving crystal/liquid interface [9]: the first flux is from the liquid to the crystal per unit time at a single kink or atomic micro-roughness, and the second one is from the crystal to the liquid. This results in the non-zero interface velocity

$$V = k_T^{(M)}(T)\left[1 - \exp\left(\frac{-\Delta G}{k_B T}\right)\right], \tag{A 1}$$

where $k_B$ is the Boltzmann constant and $T$ is the absolute temperature. The temperature-dependent kinetic coefficient $k_T^{(M)}$ in equation (A 1) can be found from various atomistic theories adapted to the concrete growth mechanism of crystals.

In the present work, we refer to theories describing the collision limited mechanism as formulated by Broughton, Gilmer and Jackson [74] and the diffusion limited mechanism as analysed by Wilson & Frenkel [75,76]. These theories summarize the kinetic coefficients as

$$k_T^{(M)}(T) = \begin{cases} k_T^{(\mathrm{CLT})} = \dfrac{a}{\lambda}\sqrt{\dfrac{3k_B T}{m}} f_0, \\ k_T^{(\mathrm{DLT})} = \dfrac{D(T)a}{\lambda^2} f_0 \exp\left(\dfrac{-\Delta H_f}{k_B T}\right), \end{cases} \tag{A 2}$$

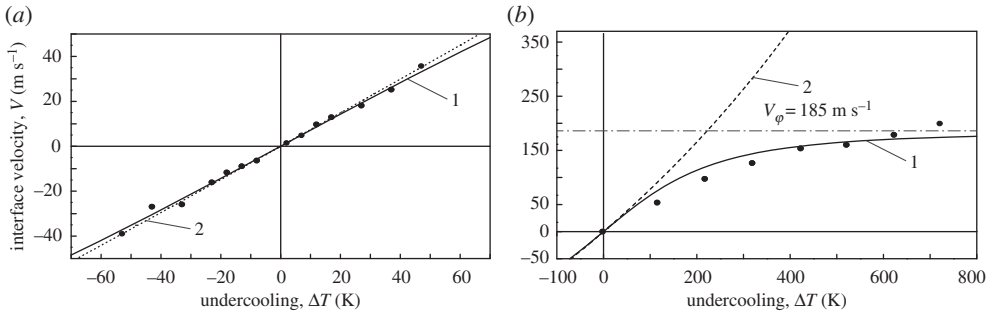


**Figure 5.** Velocity of crystal growth versus kinetic undercooling at a planar solid/liquid interface [53]. (*a*) Comparison of the predicted interface velocity $V$ by equations (A 1) and (A 2) (dotted line, curve 2) of the diffusion limited growth ('M=DLT') and by equation (B 17) (solid line, curve 1) of the Phase Field Model (PFM) with data of molecular dynamics simulations (full circles) obtained by Mendelev *et al.* [78] for Ni in the case of low undercoolings $0 < \Delta T$ (K) $< 50$ and superheatings $-55 < \Delta T$ (K) $< 0$, respectively. (*b*) Comparison of the predicted interface velocity $V$ by equations (A 1) and (A 2) (dashed line, curve 2) of diffusion limited growth ('M=DLT') and by equation (B 17) (solid line, curve 1) of the PFM with data of molecular dynamics simulations (full circles) after Hoyt *et al.* [80] for Ni in the case of large undercoolings $0 < \Delta T$ (K) $< 710$. The solid curve is limited by the maximum speed of the phase field propagation (dash-dotted line) which is $V = V_\phi = 185$ (m s$^{-1}$) for growing Ni crystals.

with the superscript 'M' corresponding to 'CLT' in the collision limited theory or 'DLT' in the diffusion limited theory, $\lambda$ is the displacement during crystallization which is proportional to the lattice parameter $a$, $m$ is the atomic mass, $f_0$ the fraction of liquid atom collisions with the solid which result in a crystallization event, $\Delta H_f$ the melting enthalpy, $D(T)$ the diffusion coefficient taken as [9] $D(T) = a^2\widetilde{\nu}\exp\left[-\Delta E_B/(k_BT)\right]$, $\widetilde{\nu}$ the frequency of thermal vibrations of an atom (assumed as equal in the crystal and the liquid for the sake of simplicity), $E_B$ the activation energy for diffusion, $\exp[-\Delta H_f/(k_BT)]$ the probability of finding an atom of the liquid in the immediate vicinity of the kink on the crystal surface in the most advantageous activation complex corresponding to the barrier $E_B$.

Using the approximation $\Delta G \ll k_BT$

$$\Delta G = \frac{\Delta H_f(-\Delta T_K)}{T_m}, \quad \Delta T_K = T_m - T, \tag{A 3}$$

which is adopted for a pure substance, equation (A 1) is reduced to its linear form as

$$V = \beta_K^{(M)}(T)\Delta T_K, \tag{A 4}$$

with the temperature-dependent coefficients (A 2) transforming to the kinetic coefficients of crystal growth as

$$\beta_K^{(M)} = \begin{cases} \beta_K^{(\mathrm{CLT})} = \dfrac{a}{\lambda}f_0\sqrt{\dfrac{3k_BT}{m}}\dfrac{\Delta H_f}{k_BT_m^2}, \\ \beta_K^{(\mathrm{DLT})} = \dfrac{D(T)a}{\lambda^2}\dfrac{\Delta H_f}{k_BT_m^2}f_0\exp\left(\dfrac{-\Delta H_f}{k_BT}\right), \end{cases} \tag{A 5}$$

where $T_m$ is the melting point and $\Delta T_K$ is the undercooling.

In equations (A 1)–(A 5), the diffusion limited theory takes into account the diffusion transport coefficient $D(T)$ of the bulk supercooled liquid; therefore, $k_T^{(\mathrm{DLT})}(T)$ (as well as $\beta_K^{(\mathrm{DLT})}$) exhibits a strong temperature dependence which is generally associated with thermally activated processes. Contrary to this, the collision limited theory predicts a kinetic coefficient proportional to the mean particle velocity, that is, $k_T^{(\mathrm{CLT})} \propto \sqrt{T}$ (and also $\beta_K^{(\mathrm{CLT})} \propto \sqrt{T}$) presenting the barrierless mechanism of growth. Quantitative estimations of kinetic growth coefficients for various crystal growth models can be found in [77,78] as obtained from atomistic simulations and in [79] as

obtained from experimental measurements. However, the collision limited mechanism fails in many cases of crystal growth (see, e.g. supplementary material of ref. [54]). The diffusion limited theory also has difficulties quantitatively describing the growth kinetics in a wide range of temperatures [55,77]. Figure 5 shows the results of calculations by equations (A 1) and (A 2) for Ni crystals in comparison with data of molecular dynamics simulations [78,80] (all data for the computations are given in ref. [53]). In the relatively small range of undercoolings, $0 < \Delta T_K$ (K) $< 50$, and superheatings, $-55 < \Delta T_K$ (K) $< 0$, figure 5*a* shows that MD data exhibit a linear behaviour of the interface velocity, both in melting and in crystallization, that is well described by the diffusion limited theory. For the large range of undercoolings, $0 < \Delta T_K$ (K) $< 710$, figure 5*b* shows that the equation following from the diffusion limited theory leads to inconsistent behaviour in comparison with MD data qualitatively and, as a consequence, quantitatively.

## Appendix B. Kinetic phase field model

Traditional phase field models based on the hypothesis of local thermodynamic equilibrium predict linear behaviour for the velocity, $V \propto \Delta G$, describe data of atomistic simulations at relatively small interface velocity and clearly disagree with these data for large values of driving forces [81]. Owing to today's experimentally reachable large driving forces and high growth velocities [8], a phase field model going beyond the hypothesis of local equilibrium has been formulated [82,83] which predicts linear behaviour at small driving forces and a nonlinear behaviour at large driving forces [58,84]. We reformulate and further develop this model to compare its predictions with the data of atomistic simulations exhibiting a maximum in the velocity/undercooling relationship.

In the present derivation, the so-called 'kinetic energy approach' [82,85] as defined in [86] is used. This model describes non-equilibrium effects appearing in rapid solidification, in particular, non-equilibrium solute trapping with a transition to diffussionless crystal growth kinetics [87].

Consider a binary mixture consisting of solvent and solute undergoing a phase transition, particularly solidification/melting, from the undercooled/overheated state, for which the free energy is described by

$$\mathcal{G} = \int_{v_0} \left[ \frac{\varepsilon_\phi^2}{2} |\nabla \phi|^2 + G\left(T, C, \phi, \frac{\partial \phi}{\partial t}\right) \right] \mathrm{d}v_0, \tag{B 1}$$

where $v_0$ is the volume of the mixture, $\varepsilon_\phi^2$ is the gradient energy coefficient related to the interface energy $\gamma$, $\phi$ is the phase field variable defined as $\phi = 0$ in the liquid phase and $\phi = 1$ in the solid phase, $\partial\phi/\partial t$ is the gradient flow for the phase field and $C$ is the solute concentration. Introducing the phase field $\phi$ and gradient flow $\partial\phi/\partial t$ as independent thermodynamic variables in the Gibbs potential, $G(T, C, \phi, \partial\phi/\partial t)$ can be considered to be fully analogous to Newtonian mechanics where the initial position and velocity of a particle must be specified to determine their evolution and velocity. Indeed, if inertial effects are sufficiently low in comparison with dissipative effects during phase field propagation, $\partial\phi/\partial t$ will be directly determined by a dynamical equation in terms of $\phi$ and its gradient. Otherwise, $\phi$ and $\partial\phi/\partial t$ will be independent and an equation for $\partial^2\phi/\partial t^2$ must be found [82].

The Gibbs potential $G(T, C, \phi, \partial\phi/\partial t)$ is given by [88]

$$G(T, C, \phi) = G_{\mathrm{eq}}(T, C, \phi) + G_{\mathrm{neq}}\left(T, \frac{\partial \phi}{\partial t}\right), \tag{B 2}$$

with the local equilibrium contribution

$$G_{\mathrm{eq}}(T, C, \phi) = [1 - p(\phi)]G_l(T, C) + p(\phi)G_s(T, C) + W_\phi(T, C)g(\phi), \tag{B 3}$$

and the local non-equilibrium contribution

$$G_{\mathrm{neq}}\left(T, \frac{\partial \phi}{\partial t}\right) = \frac{\alpha_\phi(T)}{2}\left(\frac{\partial \phi}{\partial t}\right)^2. \tag{B 4}$$

The contributions equations (B 3) and (B 4) include the interpolation function $p(\phi)$ and the double-well function $g(\phi)$ defined by [89]

$$p(\phi) = (3 - 2\phi)\phi^2 \quad \text{and} \quad g(\phi) = (1 - \phi)^2\phi^2, \tag{B 5}$$

the barrier $W_\phi(T, C)$ between the phases and the phenomenological coefficients $\alpha_\phi(T)$ being proportional to the relaxation time $\tau_\phi$ of the gradient flow $\partial\phi/\partial t$. The local non-equilibrium contribution equation (B 4) can be considered a kinetic energy term added to the Gibbs potential in the traditional phase field theory. Attempts to introduce such a kinetic term was made earlier in the theory of adsorption of sound in liquids [90] or in the theory of kink propagation [91]. Using the formalism of EIT [32], the gradient flow $\partial\phi/\partial t$ is introduced as an independent thermodynamic variable that yields the kinetic energy equation (B 4) naturally [92].

A stable evolution of the entire system is given by the Lyapunov condition of a non-positive change of the total Gibbs free energy with time. For the functional equation (B 1), this condition is given by the non-strict inequality [88]

$$\frac{\mathrm{d}\mathcal{G}}{\mathrm{d}t} = \frac{\mathrm{d}}{\mathrm{d}t}\int_{v_0}\left[\frac{\varepsilon_\phi^2}{2}|\nabla\phi|^2 + G\left(T, C, \phi, \frac{\partial\phi}{\partial t}\right)\right]\mathrm{d}v_0 \le 0, \tag{B 6}$$

from which one finds the following phase field equation [84]

$$\tau_\phi\frac{\partial^2\phi}{\partial t^2} + \frac{\partial\phi}{\partial t} = D_\phi\nabla^2\phi - M_\phi\left[\Delta G\frac{\mathrm{d}p(\phi)}{\mathrm{d}\phi} + W_\phi(T, C)\frac{\mathrm{d}g(\phi)}{\mathrm{d}\phi}\right], \tag{B 7}$$

where the Gibbs free energy difference $\Delta G$ is given by

$$\Delta G = G_s(T, C) - G_l(T, C)\begin{cases} < 0, & \text{solidification,} \\ > 0, & \text{melting.} \end{cases} \tag{B 8}$$

The variety of transformations are obtained for different temperature approximations [57], dilute mixtures [93] and thermodynamic functions from data bases [94,95]. The diffusion coefficient of the phase field

$$D_\phi(T) = \varepsilon_\phi^2 M_\phi(T) \tag{B 9}$$

essentially depends on the temperature, if the phase transition is considered in a wide temperature range [58].

The hyperbolic equation (B 7) describes the relaxation of two variables: relaxation of the slow $\phi$-field by the first time derivative and relaxation of the gradient flow $\partial\phi/\partial t$ by the second time derivative. In this sense, due to introducing the relaxation of $\partial\phi/\partial t$, equation (B 7) describes the evolution of the local non-equilibrium system. In a general case, this equation should be solved numerically using specially developed algorithms [88,96,97]. Further, we show the importance of using the gradient flow relaxation and, consequently, the role of local non-equilibrium in rapid crystal growth kinetics using a travelling wave analytical solution.

In equilibrium, $\Delta G = 0$, $G_s(T, C) = G_l(T, C)$, equation (B 7) allows a single dimensionally steady solution at $\partial\phi/\partial t = 0$ along the spatial $x$-axis:

$$\phi(x) = \frac{1}{2}\left[1 - \tanh\left(\frac{x}{\delta_I}\right)\right] \quad \text{within the diffuse interface} \quad -\frac{\delta_I}{2} < x < +\frac{\delta_I}{2}, \tag{B 10}$$

with the stationary width of diffuse interface

$$\delta_I = \frac{\sqrt{2}\varepsilon_\phi}{\sqrt{W_\phi(T, C)}}, \tag{B 11}$$

and with the boundary conditions $\phi = 1$ as $x \le \delta_I$ and $\phi = 0$ as $x \ge \delta_I$. Then, the surface energy $\gamma$ of the crystal/liquid interface is given by

$$\gamma = \int_{-\infty}^{+\infty}\left[\frac{\varepsilon_\phi^2}{2}\left(\frac{\mathrm{d}\phi}{\mathrm{d}x}\right)^2 + W_\phi(T, C)g(\phi)\right]\mathrm{d}x = \frac{\varepsilon_\phi\sqrt{W_\phi(T, C)}}{3\sqrt{2}} = \frac{\delta_I W_\phi(T, C)}{6}. \tag{B 12}$$

In the dynamics, $\Delta G = G_s(T,C) - G_l(T,C) \neq 0$, equation (B 7) has one dimensional travelling wave solution [84,87]

$$\phi(x,t) = \frac{1}{2}\left[1 - \tanh\left(\frac{x - Vt}{\ell}\right)\right], \tag{B 13}$$

with the boundary conditions $\phi \to 1$ as $x - Vt \to -\infty$ and $\phi \to 0$ as $x - Vt \to +\infty$, with the constant velocity $V$ limited by $V_\phi$ as a maximum speed of phase field propagation

$$V = \frac{\mu_k}{\Delta H_f}\frac{-\Delta G}{\sqrt{1 + \left(\mu_k \Delta G/\Delta H_f V_\phi\right)^2}}, \tag{B 14}$$

the velocity-corrected effective interface thickness

$$\ell = \frac{2\delta_I}{3}\left[1 - \frac{V^2}{V_\phi^2}\right]^{1/2}, \tag{B 15}$$

and the mobility $M_\phi$ related to the interface kinetic coefficient $\mu_k$ as

$$\mu_k = \frac{18\gamma}{W_\phi(T,C)} M_\phi(T)\Delta H_f. \tag{B 16}$$

*First*, the particular solution equation (B 13) with the hyperbolic tangent function follows from the general set of analytical solutions of Allen–Cahn-type equations [98,99] which is given in the present model by equation (B 7). *Second*, the interface velocity, $V$, cannot exceed the maximum speed of disturbance propagation in the phase field, because the phase field itself dictates the interface shape and its velocity, i.e. $V < V_\phi$ in the solutions equations (B 13)–(B 15). *Third*, with regard to the effective interface thickness (B 15), one has to note two important issues:

(i) with increasing interface velocity, $\ell$ should become smaller than the constant interface width $\delta_I$ that has been chosen as a reference for the interface thickness in equilibrium state, equation (B 11);
(ii) within the limit $V \to V_\phi$, one gets $\ell \to 0$, therefore, the phase field variation will be steeper with the tendency to build up a sharp interface as the velocity increases.

Using equations (B 12) and (B 16), the crystal growth velocity (B 14) can be re-written as

$$V = \frac{-D_\phi(\Delta T_K)\Delta G(\Delta T_K)}{\gamma\sqrt{1 + \left[(D_\phi(\Delta T_K)/\gamma V_\phi(\Delta T_K))\Delta G(\Delta T_K)\right]^2}}, \tag{B 17}$$

where the diffusive motion of the phase field is dictated by the temperature-dependent coefficient equation (B 9). At small and moderate driving forces, $D_\phi \Delta G/\gamma \ll V_\phi$, the interface velocity is linearly proportional to the difference of the free energy, i.e. $V \propto \Delta G$. At large driving forces, when $D_\phi \Delta G/\gamma$ is of the order of $V_\phi$, the square root $\sqrt{1 + [D_\phi \Delta G/(\gamma V_\phi)]^2}$ in equation (B 17) causes nonlinearity of the velocity. This square root appears in equation (B 17) due to taking into account the local non-equilibrium effect in the form of the relaxation of the gradient flow, $\partial\phi/\partial t$, which results in the second derivative $\partial^2\phi/\partial t^2$ in the dynamic equation (B 7).

The quantitative comparison, figure 5*a*, shows that in the range of small undercoolings, $0 < \Delta T_K(\mathrm{K}) < 50$, and superheating, $-55 < \Delta T_K(\mathrm{K}) < 0$, equation (B 17) predicts linear kinetics for growing/melting Ni crystals, $V \propto \Delta T_K$. This is well modelled by the molecular dynamics simulations in [78] and is in confluence with the kinetic behaviour described by the diffusion limited theory, equations (A 1)–(A 5) with 'M=DLT'.

For the large range of undercoolings, $0 < \Delta T_K$ (K) $< 710$, figure 5*b* shows that equation (B 17) predicts a gradual deviation of the velocity $V$ from the linear behaviour as the undercooling

increases. Such behaviour in crystal growth kinetics has been found by molecular dynamics simulations of elemental systems [80,100], qualitatively confirmed in [84] and quantitatively confirmed in [53]. These qualitative and quantitative deviations are due to the existence of the square root $\sqrt{1+[D_\phi \Delta G/(\gamma V_\phi)]^2}$ in equation (B 17). Because this square root appears as a consequence of the local relaxation to equilibrium, the quantitative comparison shows the importance and usefulness of the local non-equilibrium effect in the dynamics of a phase field at large driving forces.

## References


1. Lavernia EJ, Srivatsan TS. 2010 The rapid solidification processing of materials: science, principles, technology, advances, and applications. *J. Mater. Sci.* **45**, 287–325. (doi:10.1007/s10853-009-3995-5)
2. Herlach DM, Matson DM. 2012 *Solidification of containerless undercooled melts*. Weinheim, Germany: Wiley-VCH.
3. Jones H. 1973 Splat cooling and metastable phases. *Rep. Prog. Phys.* **36**, 1425–1497. (doi:10.1088/0034-4885/36/11/002)
4. Miroshnichenko IS. 1982 *Quenching from the liquid state*. Moscow, Russia: Metallurgia.
5. Feuerbacher B. 1989 Phase formation in metastable solidification of metals. *Mat. Sci. Eng. Rep.* **40**, 1–40. (doi:10.1016/S0920-2307(89)80008-8)
6. Herlach DM, Cochrane RF, Egry I, Fecht HJ, Greer AL. 1993 Containerless processing in the study of metallic melts and their solidification. *Inter. Mater. Rev.* **38**, 273–347. (doi:10.1179/095066093790326267)
7. Herlach D. 1994 Non-equilibrium solidification of undercooled metallic melts. *Mat. Sci. Eng. Rep.* **12**, 177–272. (doi:10.1016/0927-796x(94)90011-6)
8. Herlach DM, Galenko PK, Holland-Moritz D. 2007 *Metastable solids from undercooled melts*. Amsterdam, The Netherlands: Elsevier.
9. Chernov AA. 1984 *Modern crystallography III. Crystal growth*. Berlin, Germany: Springer.
10. Baker JC, Cahn JW. 1969 Solute trapping by rapid solidification. *Acta Metal.* **17**, 575–578. (doi:10.1016/0001-6160(69)90116-3)
11. Baker JC, Cahn JW. 1971 Thermodynamics of solidification, ch. 2. In *Solidification* (eds TJ Hughel, GF Bolling), pp. 23–58. OH, US: ASM Metals Park.
12. Boettinger WJ, Coriell SR. 1986 Microstructure formation in rapidly solidified alloys. In *Science and technology of the undercooled melting* (eds PR Sahm, H Jones, CM Adam). Dordrecht, The Netherlands: Martinus Nijhoâ.
13. Kurz W, Fisher DJ. 1989 *Fundamentals of solidifification*, 4th edn. Aedermannsdorf, Switzerland: Trans Tech.
14. Aziz MJ, Kaplan T. 1988 Continuous growth model for interface motion during alloy solidification. *Acta Metal.* **36**, 2335–2347. (doi:10.1016/0001-6160(88)90333-1)
15. Biloni H, Boettinger WJ. 1996 Solidification. In *Physical metallurgy* (eds RW Cahn, P Haasen), ch. 8, vol. I. Amsterdam, The Netherlands: Elsevier.
16. Hillert M, Rettenmayr M. 2003 Deviation from local equilibrium at migrating phase interfaces. *Acta Mater.* **51**, 2803–2809. (doi:10.1016/S1359-6454(03)00085-5)
17. Galenko P. 2002 Extended thermodynamical analysis of a motion of the solid-liquid interface in a rapidly solidifying alloy. *Phys. Rev. B* **65**, 144103-1–144103-11. (doi:10.1103/PhysRevB.65.144103)
18. Galenko PK, Jou D. 2019 Rapid solidification as non-ergodic phenomenon. *Phys. Rep* (Unpublished manuscript)
19. Galenko PK, Danilov DA. 1997 Local nonequilibrium effect on rapid dendritic growth in a binary alloy melt. *Phys. Lett. A* **235**, 271–280. (doi:10.1016/s0375-9601(97)00562-8)
20. Galenko PK, Danilov DA. 1999 Model for free dendritic alloy growth under interfacial and bulk phase nonequilibrium conditions. *J. Cryst. Growth* **197**, 992–1002. (doi:10.1016/s0022-0248(98)00977-4)
21. Galenko PK, Reutzel S, Herlach DM, Danilov D, Nestler B. 2007 Modelling of dendritic solidification in undercooled dilute NiZr melts. *Acta Mater.* **55**, 6834–6842. (doi:10.1016/j.actamat.2007.08.038)

22. Hartmann H, Galenko PK, Holland-Moritz D, Kolbe M, Herlach DM, Shuleshova O. 2008 Nonequilibrium solidification in undercooled $Ti_{45}Al_{55}$ melts. *J. Appl. Phys.* **103**, 073509-1–073509-9. (doi:10.1063/1.2903920)
23. Galenko PK, Reutzel S, Herlach DM, Fries SG, Steinbach I, Apel M. 2009 Dendritic solidification in undercooled Ni-Zr-Al melts: experiments and modeling. *Acta Mater.* **57**, 6166–6175. (doi:10.1016/j.actamat.2009.08.043)
24. Hartmann H, Holland-Moritz D, Galenko PK, Herlach DM. 2009 Evidence of the transition from ordered to disordered growth during rapid solidification of an intermetallic phase. *Europhys. Lett.* **87**, 40007-1–40007-6. (doi:10.1209/0295-5075/87/40007)
25. Galenko PK, Nizovtseva IG, Reuther K, Rettenmayr M. 2018 Kinetic transition in the order–disorder transformation at a solid/liquid interface. *Phil. Trans. R. Soc. A* **376**, 20170207. (doi:10.1098/rsta.2017.0207)
26. Skripov VP, Koverda VP. 1984 *Spontaneous crystallization of supercooled liquids*. Moscow, Russia: Nauka.
27. Wang Q, Wang LM, Ma MZ, Binder S, Volkmann T, Herlach DM, Wang JS, Xue QG, Tian YJ, Liu RP. 2011 Diffusion-controlled crystal growth in deeply undercooled melt on approaching the glass transition. *Phys. Rev. B* **83**, 014202-1–014202-5. (doi:10.1103/PhysRevB.83.014202)
28. Orava J, Greer AL. 2014 Fast and slow crystal growth kinetics in glass-forming melts. *J. Chem. Phys.* **140**, 214504. (doi:10.1063/1.4880959)
29. Wang H, Herlach DM, Liu RP. 2014 Dendrite growth in $Cu_{50}Zr_{50}$ glass-forming melts, thermodynamics vs. kinetics. *Europhys. Lett.* **105**, 36001. (doi:10.1209/0295-5075/105/36001)
30. Boettinger WJ, Coriell SR, Sekerka RF. 1984 Mechanisms of microsegregation-free solidification. *Mat. Sci. Eng.* **65**, 27–36. (doi.org/10.1016/0025-5416(84)90196-4)
31. Jou D, Casas-Vazquez J, Lebon G. 1999 Extended irreversible thermodynamics revisited (1988–98). *Rep. Prog. Phys.* **62**, 1035. (doi:10.1088/0034-4885/62/7/201)
32. Jou D, Casas-Vazquez J, Lebon G. 2010 *Extended irreversible thermodynamics*, 4th edn. Berlin, Germany: Springer.
33. Galenko PK, Danilov DA, Alexandrov DV. 2015 Solute redistribution around crystal shapes growing under hyperbolic mass transport. *Int. J. Heat. Mass Trans.* **89**, 1054–1060. (doi:10.1016/j.ijheatmasstransfer.2015.06.011)
34. Galenko PK, Herlach DM. 2006 Suppression of eutectic precipitation in rapid solidification of a binary system. In *Spring-Meeting of the German Physical Society (DPG). Proc. of the DPG-Conf., Dresden, Germany, 27–31 March*, p. 563. Dresden, Germany: Deutsche Physikalische Gesellschaft.
35. Galenko PK, Jou D. 2010 Thermodynamics and kinetics of fast spinodal decomposition controlled by diffusion in the presence of fluctuations. *Solid-solid phase transformations in inorganic materials. Proc. of PTM-Conf. Avignon, France, 6–11 June*, p. 37. Zürich-Dürnten, Switzerland: Trans Tech Publications.
36. Masato D, Sorgato M, Lucchetta G. 2017 Prototyping and modeling of the centrifugal casting process for paraffin waxes. *Mater. Manufact. Proc.* **32**, 1823–1830. (doi:10.1080/10426914.2017.1317791)
37. Alexandrov DV, Galenko PK. 2013 Selection criterion for the growing dendritic tip at the inner core boundary. *J. Phys. A: Math. Theor.* **46**, 195101-1–195101-12. (doi:10.1088/1751-8113/46/19/195101)
38. Zhuravlev VA. 2006 *Solidification and crystallization of alloys with hetero-trasformations*. Izhevsk, Russia: Regular and Chaotic Dynamics.
39. Glicksman ME. 2011 *Principles of solidification: an introduction to modern casting and crystal growth concepts*. New York, NY: Springer.
40. Alexandrov DV, Danilov DA, Galenko PK. 2016 Selection criterion of a stable dendrite growth in rapid solidification. *J. Heat Mass Trans.* **101**, 789–799. (doi:10.1016/j.ijheatmasstransfer.2016.05.085)
41. Alexandrov DV, Galenko PK. 2017 Selected mode for rapidly growing needle-like dendrite controlled by heat and mass transport. *Acta Mater.* **137**, 64–70. (doi:10.1016/j.actamat.2017.07.022)
42. Barbieri A, Langer JS. 1989 Predictions of dendritic growth rates in the linearized solvability theory. *Phys. Rev. A* **39**, 5314–5325. (doi:10.1103/PhysRevA.39.5314)
43. Amar MB, Pelcé P. 1989 Impurity effect on dendritic growth. *Phys. Rev. A* **39**, 4263–4269. (doi:10.1103/PhysRevA.39.4263)

44. Brener E, Mel'nikov VI. 1990 Two-dimensional dendritic growth at arbitrary Peclet number. *J. Phys. Fran.* **51**, 157–166. (doi:10.1051/jphys:01990005102015700)
45. Müller-Krumbhaar H, Abel T, Brener E, Hartmann M, Eissfeldt N, Temkin D. 2002 Growth-morphologies in solidification and hydrodynamics. *JSME Inter. J. B* **45**, 129–132. (doi:10.1299/jsmeb.45.129)
46. Trivedi R, Kurz W. 1986 Morphological stability of a planar interface under rapid solidification conditions. *Acta Metal.* **34**, 1663–1670. (doi:10.1016/0001-6160(86)90112-4)
47. Trivedi R, Kurz W. 1994 Dendritic growth. *Inter. Mat. Rev.* **39**, 49–74. (doi:10.1179/imr.1994.39.2.49)
48. Alexandrov DV, Galenko PK. 2017 Selected mode of dendritic growth with n-fold symmetry in the presence of a forced flow. *Europhys. Lett.* **119**, 1600-1–1600-17. (doi:10.1209/0295-5075/119/16001)
49. Alexandrov DV, Galenko PK, Toropova LV. 2018 Thermo-solutal and kinetic modes of stable dendritic growth with different symmetries of crystalline anisotropy in the presence of convection. *Phil. Trans. R. Soc. A* **376**, 20170215-1. (doi:10.1098/rsta.2017.0215)
50. Binder S, Galenko PK, Herlach DM. 2014 The effect of fluid flow on the solidification of $Ni_2B$ from the undercooled melt. *J. Appl. Phys.* **115**, 053511-1–053511-11. (doi:10.1063/1.4864151)
51. Galenko PK, Danilov DA. 2000 Steady-state shapes of growing crystals in the field of local nonequilibrium diffusion. *Phys. Lett. A* **272**, 207–217. (doi:10.1016/S0375-9601(00)00417-5)
52. Chernov AA. 1968 Kinetic phase transitions. *Soviet Phys. JETP* **26**, 1182–1190.
53. Salhoumi A, Galenko PK. 2017 Analysis of interface kinetics: solutions of the Gibbs-Thomson-type equation and of the kinetic rate theory. *IOP Conf. Ser.: Mat. Sc. Eng.* **192**, 12014. (doi:10.1088/1757-899X/192/1/012014)
54. Tang C, Harrowell P. 2013 Anomalously slow crystal growth of the glass-forming alloy CuZr. *Nat. Mat.* **12**, 507. (doi:10.1038/NMAT3631)
55. Kerrache A, Horbach J, Binder K. 2008 Molecular-dynamics computer simulation of crystal growth and melting in $Al_{50}Ni_{50}$. *Europhys. Lett.* **81**, 58001. (doi:10.1209/0295-5075/81/58001)
56. Chan WL, Averback RS, Cahill DG, Ashkenazy Y. 2009 Solidification velocities in deeply undercooled silver. *Phys. Rev. Lett.* **102**, 095701. (doi:10.1103/PhysRevLett.102.095701)
57. Thompson CV, Spaepen F. 1979 On the approximation of the free energy change on crystallization. *Acta Metal.* **27**, 1855–1859.
58. Novokreshchenova AA, Lebedev VG. 2017 Determining the phase-field mobility of pure nickel based on molecular dynamics data. *Tech. Phys.* **62**, 642–644. (doi:10.1134/S1063784217040181)
59. Garca-Coln LS, Del Castillo LF, Goldstein P. 1989 Theoretical basis for the Vogel-Fulcher-Tammann equation. *Phys. Rev. B* **40**, 7040–7044. (doi:10.1103/PhysRevB.40.7040)
60. Galenko PK, Hanke R, Paul P, Koch S, Rettenmayr M, Gegner J, Herlach DM, Dreier W, Kharanzhevski EV. 2017 Solidification kinetics of a Cu-Zr alloy: ground-based and microgravity experiments. *IOP Conf. Ser.: Mat. Sc. Eng.* **192**, 012028. (doi:10.1088/1757-899X/192/1/012028)
61. Chan WL, Averback RS, Cahill DG, Ashkenazy Y. 2009 Solidification Velocities in Deeply Undercooled Silver. *Phys. Rev. Lett.* **102**, 095701. (doi:10.1103/PhysRevLett.102.095701)
62. Hanke R, Koch S, Kobold R, Paul P, Galenko PK, Herlach DM, Rettenmayr M. 2017 Parabolic flight experiment on TEMPUS 2016 within the MULTIPHAS-project: Measurement of solidification velocity in $Zr_{50}Cu_{30}Ni_{20}$. *Presentation on the Int. Working Group Meeting in German Aerospace Center (DLR-Bonn), Bonn-Bad-Godesberg, Germany, 15–16 March*. Bonn, Germany: Deutsches Zentrum für Luft- und Raumfahrt.
63. Kobold R. 2016 Crystal growth in undercooled melts of glass forming Zr-based alloys. PhD thesis, Ruhr-Universitat Bochum, Germany, p. 170.
64. Soklaski R, Nussinov Z, Markow Z, Kelton KF, Yang L. 2013 Connectivity of the icosahedral network and a dramatically growing static length scale in Cu-Zr binary metallic glasses. *Phys. Rev. B* **87**, 184203. (doi:10.1103/PhysRevB.87.184203)
65. Boettinger WJ, Aziz MJ. 1989 Theory for the trapping of disorder and solute in intermetallic phases by rapid solidification. *Acta Metall.* **37**, 3379-3391. (doi: 10.1016/0001-6160(89)90210-1)
66. Barth M, Wei B, Herlach DM. 1995 Crystal growth in undercooled melts of the intermetallic compounds FeSi and CoSi. *Phys. Rev. B* **51**, 3422–3428. (doi:10.1103/PhysRevB.51.3422)
67. Greer AL, Assadi H. 1997 Rapid solidification of intermetallic compounds. *Mater.Sci. Eng. A* **226-228**, 133–141. (doi:10.1016/S0921-5093(97)80026-3)

68. Hartmann H, Holland-Moritz D, Galenko PK, Herlach DM. 2009 Evidence of the transition from ordered to disordered growth during rapid solidification of an intermetallic phase. *Europhys. Lett.* **87**, 40 007–40 013. (doi: 10.1209/0295-5075/87/40007)
69. Yang C, Gao J. 2014 Dendritic growth kinetics and disorder trapping of the intermetallic compound $Ni_3Sn$ under a static magnetic field. *J. Cryst. Growth* **394**, 24–27. (doi: 10.1016/j.jcrysgro.2014.02.015)
70. Holland-Moritz D, Yang F, Kordel T, Klein S, Kargl F, Gegner J, Hansen T, Bednarcik J, Kaban I, Shuleshova O, Mattern N, Meyer A. 2012 Does an icosahedral short-range order prevail in glass-forming Zr-Cu melts? *Europhys. Lett.* **100**, 56 002–56 000. (doi:10.1209/0295-5075/100/56002)
71. Yang F, Holland-Moritz D, Gegner J, Heintzmann P, Kargl F, Yuan CC, Simeoni GG, Meyer A. 2014 Atomic dynamics in binary Zr-Cu liquids. *Europhys. Lett.* **107**, 46001. (doi:10.1209/0295-5075/107/46001)
72. Gegner J, Shuleshova O, Kobold R, Holland-Moritz D, Herlach DM. 2013 In situ observation of the phase selection from the undercooled melt in Cu-Zr. *J. Alloys Compd.* **576**, 232. (doi:10.1016/j.jallcom.2013.04.035)
73. Christian JW. 1975 *The theory of transformations in metals and alloys*. Oxford, UK: Pergamon.
74. Broughton JQ, Gilmer GH, Jackson KA. 1982 Crystallization rates of a Lennard-Jones liquid. *Phys. Rev. Lett.* **49**, 1496. (doi:10.1103/PhysRevLett.49.1496)
75. Wilson HA. 1900 On the velocity of solidification and viscosity of supercooled liquids. *Phil. Mag.* **50**, 238.
76. Frenkel J. 1946 *Kinetic theory of solids*. New York, NY: Oxford University Press.
77. Ashkenazy Y, Averback RS. 2007 Atomic mechanisms controlling crystallization behaviour in metals at deep undercoolings. *Europhys. Lett.* **79**, 26005-1–26005-6. (doi:10.1209/0295-5075/79/26005)
78. Mendelev MI, Rahman MJ, Hoyt JJ, Asta M. 2010 Molecular-dynamics study of solid-liquid interface migration in fcc metals. *Mod. Simul. Mat. Sc. Eng.* **18**, 074002-1–074002-18. (doi:10.1088/0965-0393/18/7/074002)
79. Herlach DM, Simons D, Pichon PY. 2018 Crystal growth kinetics in undercooled melts of pure Ge, Si and Ge-Si alloys. *Phil. Trans. R. Soc. A* **376**, 20170205-1–20170205-13. (doi:10.1098/rsta.2017.0205)
80. Hoyt JJ, Sadigh B, Asta M, Foiles SM. 1999 Kinetic phase field parameters for the Cu-Ni system derived from atomistic computations. *Acta Mater.* **47**, 3181–3187. (doi:10.1016/S1359-6454(99)00189-5)
81. Berghoff M, Selzer M, Nestler B. 2013 Phase-field simulations at the atomic scale in comparison to molecular dynamics. *Sci. World J.* **2013**, 564272. (doi:10.1155/2013/564272)
82. Galenko P, Jou D. 2005 Diffuse-interface model for rapid phase transformations in nonequilibrium systems. *Phys. Rev. E* **71**, 046125-1–046125-13. (doi:10.1103/PhysRevE.71.046125)
83. Galenko P, Danilov D, Lebedev V. 2009 Phase-field-crystal and Swift-Hohenberg equations with fast dynamics. *Phys. Rev. E* **79**, 051110-1–051110-11. (doi:10.1103/PhysRevE.79.051110)
84. Salhoumi A, Galenko PK. 2016 Gibbs-Thomson condition for the rapidly moving interface in a binary system. *Physica A* **447**, 161–171. (doi:10.1016/j.physa.2015.12.042)
85. Galenko P, Jou D. 2009 Kinetic contribution to the fast spinodal decomposition controlled by diffusion. *Physica A* **388**, 3113–3123. (doi:10.1016/j.physa.2009.04.003)
86. Wang H, Galenko PK, Zhang X, Kuang W, Liu F, Herlach DM. 2015 Phase-field modeling of an abrupt disappearance of solute drag in rapid solidification. *Acta Mater.* **90**, 282–291. (doi:10.1016/j.actamat.2015.02.021)
87. Galenko PK, Abramova EV, Jou D, Danilov DA, Lebedev VG, Herlach DM. 2011 Solute trapping in rapid solidification of a binary dilute system: a phase-field study. *Phys. Rev. E* **84**, 041143-1–041143-17. (doi:10.1103/PhysRevE.84.041143)
88. Lebedev V, Sysoeva A, Galenko P. 2011 Unconditionally gradient-stable computational schemes in problems of fast phase transitions. *Phys. Rev. E* **83**, 026705-1–026705-11. (doi:10.1103/PhysRevE.83.026705)
89. Wang SL, Sekerka RF, Wheeler AA, Murray BT, Coriell SR, Braun RJ, McFadden GB. 1993 Thermodynamically-consistent phase-field models for solidification. *Physica D* **69**, 189–200. (doi:10.1016/0167-2789(93)90189-8)

90. Mandel'shtam LI, Leontovich MA. 1937 On the theory of sound absorption in fluids. *Zh. Eksperim. i Theor.* **7**, 438–449.
91. Chaikin PM, Lubensky TC. 1995 *Principles of condensed matter physics*. Cambridge, UK: Cambridge University Press.
92. Danilov DA, Lebedev VG, Galenko PK. 2014 A grand potential approach to phase field modeling of rapid solidification. *J. Non-Equilib. Thermodyn.* **39**, 93–111. (doi:10.1515/jnetdy-2013-0032)
93. Echebarria B, Folch R, Karma A, Plapp M. 2004 Quantitative phase-field model of alloy solidification. *Phys. Rev. E* **70**, 061604. (doi:10.1103/PhysRevE.70.061604)
94. Dinsdale AT. 1991 SGTE data for pure elements. *CALPHAD* **15**, 317–425. (doi:10.1016/0364-5916(91)90030-N)
95. Samal S, Phanikumar G. 2015 Phase evolution in hypereutectic $Al_{90}Cu_{10-x}Ni_x$ $(x = 0, 5)$ alloys. *Trans. Indian Inst. Met.* **68**, 1221. (doi:10.1007/s12666-015-0709-3)
96. Galenko PK, Gomez H, Kropotin NV, Elder KR. 2013 Unconditionally stable method and numerical solution of the hyperbolic phase-field crystal equation. *Phys. Rev. E* **88**, 013310. (doi:10.1103/PhysRevE.88.013310)
97. Bueno J, Starodumov I, Gomez H, Galenko PK, Alexandrov D. 2016 Three dimensional structures predicted by the modified phase field crystal equation. *Comp. Mater. Sci.* **111**, 310. (doi:10.1016/j.commatsci.2015.09.038)
98. Nizovtseva IG, Galenko PK, Alexandrov DV. 2016 The hyperbolic Allen-Cahn equation: exact solutions. *J. Phys. A: Math. Theor.* **49**, 435201-1–435201-14. (doi:10.1088/1751-8113/49/43/435201)
99. Nizovtseva IG, Galenko PK. 2018 Travelling-wave amplitudes as solutions of the phase-field crystal equation. *Phil. Trans. R. Soc. A* **376**, 20170202-1–20170202-15. (doi:10.1098/rsta.2017.0202)
100. Hoyt JJ, Asta M, Karma A. 2003 Atomistic and continuum modeling of denritic solidification. *Mat. Sci. Eng. R* **41**, 121–163. (doi:10.1016/S0927-796X(03)00036-6)